

pubs.acs.org/est Article

Degradation of Adsorbed Bisphenol A by Soluble Mn(III)

Yanchen Sun, Jeongdae Im, Nusrat Shobnam, Sofia K. Fanourakis, Lilin He, Lawrence M. Anovitz, Paul R. Erickson, Huihui Sun, Jie Zhuang, and Frank E. Löffler*



Cite This: Environ. Sci. Technol. 2021, 55, 13014-13023



ACCESS

III Metrics & More



Supporting Information

ABSTRACT: Bisphenol A (BPA), a high production volume chemical and potential endocrine disruptor, is found to be associated with sediments and soils due to its hydrophobicity (log $K_{\rm OW}$ of 3.42). We used superfine powdered activated carbon (SPAC) with a particle size of 1.38 \pm 0.03 μ m as a BPA sorbent and assessed degradation of BPA by oxidized manganese (Mn) species. SPAC strongly sorbed BPA, and desorption required organic solvents. No degradation of adsorbed BPA (278.7 \pm 0.6 mg BPA g⁻¹ SPAC) was observed with synthetic, solid α -MnO₂ with a particle size of 15.41 \pm 1.35 μ m; however, 89% mass reduction occurred following the addition of 0.5 mM soluble Mn(III). Small-angle neutron scattering data suggested that both

Degradation of Adsorbed Bisphenol A

Soluble Mn(III)

Micron-scale Activated Carbon

adsorption and degradation of BPA occurred in SPAC pores. The findings demonstrate that Mn(III) mediates oxidative transformation of dissolved and adsorbed BPA, the latter observation challenging the paradigm that contaminant desorption and diffusion out of pore structures are required steps for degradation. Soluble Mn(III) is abundant near oxic-anoxic interfaces, and the observation that adsorbed BPA is susceptible to degradation has implications for predicting, and possibly managing, the fate and longevity of BPA in environmental systems.

KEYWORDS: bisphenol A degradation, manganese oxides, Mn(III), MnO₂, adsorption, activated carbon, small-angle neutron scattering (SANS)

■ INTRODUCTION

Bisphenol A (BPA) is widely used in manufacturing of polycarbonate plastics, epoxy resins, flame retardants, and other products. The global BPA market was about 8 million metric tons in 2016, and a further increase is projected. BPA has been detected in numerous environmental matrices, ranging from 0.5 to 325 ng g⁻¹ (dry weight) in soil,³ 0.2 to 39.1 μ g g⁻¹ (dry weight) in dust, 4 1.49 to 13 370 ng g⁻¹ (dry weight) in sediments, and 0.5 to 776 ng L⁻¹ in surface water bodies.6 The presence of BPA in environmental systems has raised concerns due to the estrogenic properties observed in laboratory studies, 7,8 and the environmental fate of BPA is, therefore, of significant interest.9 A number of studies have reported transformation and degradation of dissolved BPA under oxic conditions by bacteria, fungi, and algae, and in addition to biotic processes, dissolved BPA is susceptible to abiotic degradation mediated by Mn(IV) dioxide mineral phases, ^{12,13} photodegradation, ¹⁴ and advanced oxidation using hydroxyl radicals.15

Following iron and titanium, manganese (Mn) is the third most abundant transition metal in the earth's crust and commonly occurs in three oxidation states, Mn(II), Mn(III), and Mn(IV), in the environment. Mn(IV) in the form of MnO₂ polymorphs is abundant in soils and sediments 17,18 and a strong oxidant ($E_{\rm H}^{\circ}_{({\rm Mn(IV)/Mn(II)})}=1.23$ V) capable of

oxidizing a variety of organic compounds, 19,20 including BPA.^{12,13} Mn(III) can be formed via the oxidation of Mn(II), 21 the one-electron reduction of Mn(IV), 22 and a conproportionation reaction between Mn(II) and Mn(IV).²³ Mn(III) is found in the minerals bixbyite (Mn_2O_3) , feitknechtite, groutite, and manganite (MnO[OH]), the mixed-charge phase hausmannite (Mn₃O₄), and in minerals with more complex chemistries. Free aqueous Mn(III) is prone to disproportionation to yield dissolved Mn(II) and solid Mn(IV) and is assumed to be short-lived in solution, which has led to a general underappreciation of Mn(III) in the traditional paradigm of Mn redox cycling.²⁴ Several studies have now demonstrated that soluble Mn(III) commonly occurs near oxic-anoxic interfaces^{25,26} and is an important environmental oxidant $(E_{\text{H}}^{\circ}_{(\text{Mn(III)}/\text{Mn(II)})} = 1.51 \text{ V})^{.27}$ Both Mn(III) and Mn(IV) are environmentally relevant oxidants, 12,27,28 but only Mn(IV) has been demonstrated to degrade BPA.

Received: June 14, 2021 Revised: August 17, 2021 Accepted: September 10, 2021 Published: September 24, 2021





With an *n*-octanol-water partition coefficient log K_{OW} of 3.42,²⁹ BPA has a tendency for sorption to hydrophobic matrices, which are major sinks for, and reservoirs of, BPA in the environment.^{3,4} Although BPA sorbed to a porous matrix is considered stable, environmental perturbations could result in the desorption and release of BPA, 30-33 thereby increasing the exposure risk. For example, the presence of co-contaminants (i.e., heavy metals), 30 elevated temperatures, 32 and elevated pH³³ has been shown to increase BPA desorption. Experiments using advanced chemical oxidation (e.g., Fenton) suggested that desorption and diffusion were required for degradation to occur, 32,34 and the fate of adsorbed BPA within porous materials is unclear. The pore structure of solid matrices characteristically contains macro- (>50 nm), meso- (2-50 nm), and micropores (<2 nm) and represents the major zones for adsorption.³⁵ Sorptive processes diminish the pore size, whereas desorption and diffusion cause the opposite effect.

Due to the widespread distribution of BPA in the environment and associated human health concerns, a detailed understanding of the fate and the longevity of BPA adsorbed to soils and sediments is needed. The objective of this study was to explore the reactivity of soluble Mn(III) toward BPA and to investigate if Mn(III) and Mn(IV) species can initiate oxidation and degradation of adsorbed BPA. To do so, we have employed small-angle neutron scattering (SANS) to quantify changes in the structure of a porous matrix following BPA sorption and treatment with oxidized Mn species. SANS is an established technique to obtain pore geometry information at a mesoscopic scale in the range of 1–100 nm and can provide information about the distribution of organic compounds within the solid matrix pore structure. 36,37

■ MATERIALS AND METHODS

Chemicals. BPA (>99% purity) was purchased from Sigma-Aldrich (St. Louis, MO, USA), and deuterated BPA-d16 (98% purity) was obtained from Cambridge Isotope Laboratories (Andover, MA, USA). Ethyl acetate, L-ascorbic acid, Leucoberbelin blue (LBB), potassium permanganate (KMnO₄), Mn(III) oxide (Mn₂O₃) (>98% purity), Mn(II) chloride tetrahydrate (MnCl₂ × 4 H₂O), and sodium pyrophosphate decahydrate (Na₄P₂O₇ × 10 H₂O) were obtained from Thermo Fisher Scientific (Waltham, MA, USA). All chemicals used were of reagent grade or higher purity. Superfine powdered activated carbon (SPAC) composed of 1.38 \pm 0.03 μ m sized activated carbon particles was obtained from REGENESIS (San Clemente, CA, USA).

Soluble Mn(III) and MnO₂ Preparation and Quantification. Soluble Mn(III) stock solutions were prepared according to an established procedure. Briefly, 8 g of Mn₂O₃ was added to 100 mL of 40 mM Na₄P₂O₇ × 10 H₂O solution and the pH was adjusted to 6.5 with 4 mM hydrochloric acid and 5 mM sodium hydroxide (NaOH). After 3 days of continuous stirring at room temperature, the mixture was centrifuged (6000g, 10 min), and the supernatant was filtered through a 0.22 μ m polyethersulfone (PES) membrane (Nalgene, Rochester, NY, USA) to remove any remaining solids.

The synthesis of MnO₂ followed a described procedure. Briefly, 2.96 g of KMnO₄ was dissolved in 74.1 mL of Milli-Q water (at least 18.2 M Ω × cm) and heated to 90 °C on a hot plate under continuous stirring. With the solution at 90 °C, 3.71 mL of 5 M NaOH was added, and then 5.56 g of MnCl₂ × 4 H₂O dissolved in 27.8 mL of Milli-Q water was slowly added.

The resulting suspension was stirred for 30 min and cooled to room temperature. The solids were collected by centrifugation at 6000g for 10 min and washed five times with Milli-Q water. The $\rm MnO_2$ precipitate was suspended in 100 mL of deoxygenated Milli-Q water.

Mn(III) concentrations were measured at 258 nm with a PerkinElmer Lambda 35 UV–vis spectrophotometer in the presence of pyrophosphate (Figure S1). A molar extinction coefficient of 6750 M^{-1} cm⁻¹ was used to calculate Mn(III) concentrations. Mn content of MnO₂ stock solutions was quantified by monitoring the absorbance following the addition of LBB at 623 nm (see the Supporting Information for details). Standard curves were prepared with LBB and KMnO₄ (Figure S2). X-ray powder diffraction (XRD) analysis was performed to confirm that the crystal structure and chemical composition of the material matched α -MnO₂ (Figure S3).

Incubation Conditions. The experiments were performed under ambient air conditions and at room temperature (\sim 21 $^{\circ}$ C), and all vessels were incubated in the dark on a rotary shaker (200 rpm, unless indicated otherwise) with the stoppers facing up.

Oxidative Transformation of BPA by Soluble Mn(III) and MnO₂. Experiments were performed in 60 mL glass serum bottles with a total volume of 40 mL of 5 mM potassium phosphate buffer, pH 7.2, containing 44 µM BPA. Sodium chloride (NaCl) was added to reach a constant ionic strength of 10 mM. The bottles were closed with black butyl rubber stoppers and agitated at 120 rpm. To test the effect of Mn on the BPA transformation rate, Mn(III) and MnO2 were added from stock solutions to achieve concentrations of 0.05, 0.1, 0.25, and 0.5 mM (nominal concentrations in the case of MnO₂). Aliquots (0.5 mL) were periodically collected after shaking and transferred to 1.5 mL plastic centrifuge tubes containing 20 μ L of L-ascorbic acid solution (5 g L⁻¹) and immediately vortexed. The samples were then centrifuged at 10 000g (Eppendorf centrifuge 5415D, Hamburg, Germany) for 5 min, and the supernatant was transferred to 2 mL glass autosampler vials. The pseudo-first-order rate constants were obtained by plotting the natural log of BPA concentrations as a function of time using five early time points, where linear relationships were observed.

Adsorption Experiments. The average size of the SPAC particles was determined by laser diffraction spectroscopy (Table S1). BPA sorption isotherms on SPAC were obtained using a batch equilibration method. 41 Briefly, 36 mg L⁻¹ (dry weight) SPAC was suspended in 5 mM phosphate buffer (pH 7.2) containing 10 mM NaCl. The adsorption experimental incubations received 1.5 mM sodium azide (NaN3) to prevent microbial growth. 42 Glass serum bottles (60 mL of the total volume) received 40 mL of the SPAC suspension and 4-40 mg L⁻¹ BPA. The bottles were closed with black butyl rubber stoppers and agitated. All experiments were performed in triplicate. Aliquots (0.5 mL) were withdrawn over time and passed through 0.2 µm BasixTM polytetrafluoroethylene (PTFE) membrane filters (Thermo Fisher Scientific, Waltham, MA, USA), and the supernatant was subjected to highperformance liquid chromatography (HPLC) analysis. The aging of adsorbed BPA was determined by measuring the extracted amount of BPA after 2, 19, 40, 50, and 60 days. The amount of BPA adsorbed onto SPAC was calculated by subtracting the aqueous phase BPA from the initial amount of BPA. The Freundlich and Langmuir isotherm models (eqs 1 and 2) were used to fit the BPA adsorption data.³²

Freundlich isotherm:

$$q_{\rm e} = k_{\rm f} \cdot C_{\rm e}^{1/n} \tag{1}$$

Langmuir isotherm:

$$q_{\rm e} = \frac{Q_0 \cdot k_{\rm L} \cdot C_{\rm e}}{1 + k_{\rm L} \cdot C_{\rm e}} \tag{2}$$

where $q_{\rm e}$ is the amount of BPA adsorbed per unit mass of SPAC at equilibrium (mg BPA g⁻¹ SPAC), $k_{\rm f}$ is a constant of the Freundlich isotherm, $C_{\rm e}$ is the liquid-phase concentration of BPA at equilibrium (mg L⁻¹), 1/n is an indicator of adsorption intensity, Q_0 is the maximum adsorption capacity (mg g⁻¹), and $k_{\rm L}$ is a constant of the Langmuir isotherm (L g⁻¹).

Desorption Kinetics. To assess the desorption kinetics, experiments were conducted with two types of SPAC with adsorbed BPA. To prepare SPAC with freshly adsorbed BPA, 1.76 µmol of BPA dissolved in 40 mL of 5 mM phosphate buffer, pH 7.2, was incubated for 0.5 h with 1.44 mg (dry weight) of SPAC in 60 mL glass serum bottles. The bottles were closed with black butyl rubber stoppers and agitated. Prolonged incubations for 60 days generated aged SPAC with adsorbed BPA. The suspensions were transferred to 50 mL Falcon conical centrifuge tubes (Thermo Fisher Scientific, Oneonta, NY, USA) and centrifuged for 15 min at 15 000g before the supernatant was carefully removed with a pipette. Each SPAC pellet was suspended in 40 mL of freshly prepared sodium phosphate buffer solution (pH 6, 7.2, and 8.2), and the suspensions were transferred to 60 mL glass serum bottles. The bottles were closed with black butyl rubber stoppers and agitated in horizontal position. Desorption experiments using fresh and aged SPAC lasted for 15 and 8 days, respectively. Suspension aliquots (0.5 mL) were withdrawn over time with plastic syringes and filtered through 0.2 µm PTFE syringe filters, and the BPA concentration in the filtrate was then measured.

Degradation of BPA Adsorbed to SPAC. Fresh and aged SPAC loaded with 278.7 \pm 0.6 mg BPA g⁻¹ were prepared to examine the degradation of adsorbed BPA by soluble Mn(III) and solid α-MnO₂. SPAC (1.44 mg) with adsorbed BPA was washed and then suspended in 40 mL of 5 mM phosphate buffer (pH 7.2) containing 10 mM NaCl, and 0.05, 0.1, 0.25, and 0.5 mM Mn(III) or 0.5 mM MnO₂ (nominal concentrations) was added to 60 mL glass serum bottles. Samples (1 mL) were withdrawn over time and extracted with ethyl acetate (see below), and BPA concentrations were determined by HPLC.

Extraction Procedures. The amount of BPA adsorbed to SPAC was measured following established liquid—liquid extraction procedures. 43,44 Each 1 mL aqueous sample was transferred to 10 mL vials, and 3 mL of ethyl acetate was added. The closed vials were agitated for 12 h and then centrifuged at 5000g for 10 min. Longer extraction periods did not increase the recovery of BPA. The organic phases from three successive extractions were combined and dried under a gentle stream of nitrogen. Each residue was dissolved in 1 mL of acetonitrile and water (1:1, v/v) and analyzed by HPLC. To test the recovery of BPA from SPAC, 1.76 μ mol of BPA was added to 60 mL serum bottles containing 1.44 mg of SPAC

suspended in 40 mL of a 5 mM phosphate buffer (pH 7.2) and agitated at 200 rpm. After 30 min, BPA was extracted with ethyl acetate as described above. All experiments were performed in triplicate, and the recovery of BPA was $101 \pm 1.3\%$

SANS Experiment and Data Analysis. SANS measures the changes in the scattering intensity as a function of scattering angle, and the comparative analysis of pore sizes derived from these data can provide information about BPA adsorption, desorption, and degradation within the SPAC pore structure. Three samples including "neat" SPAC, SPAC with adsorbed BPA, and SPAC with adsorbed BPA after the Mn(III) treatment were collected for SANS measurements. To facilitate the SANS measurements, deuterated BPA was used because its scattering length density (SLD) is very similar to that of SPAC carbon (i.e., 5.9×10^{-6} versus 6.0×10^{-6} Å⁻², respectively), and thus the scattering intensity from the SPAC/ BPA interface was expected to be very low.³⁶ Because of the contrast at this boundary, adsorption and degradation of BPA within the pores modulate the scattering intensities, and modeling of the scattering profile data can provide information about pore size changes, and thus BPA adsorption and degradation. To generate SPAC with adsorbed BPA, 880 μ mol of deuterated BPA was incubated with 1 g (dry weight) of SPAC in a total volume of 75 mL of 5 mM phosphate buffer, pH 7.2, on a rotary shaker (120 rpm) for 10 days. Preparation of SPAC samples without BPA followed identical procedures. Duplicate samples of SPAC with adsorbed deuterated BPA were analyzed with SANS to characterize the distribution of BPA within the SPAC matrix (i.e., pore size <100 nm) prior to and after treatment with 0.5 mM soluble Mn(III). To account for the effect of 2.5 mM pyrophosphate introduced with the soluble Mn(III), SPAC with adsorbed BPA was added to a solution with the same pyrophosphate concentration. All samples used in the degradation experiment were incubated on a shaker table (120 rpm) for 15 days. The three different SPAC suspensions were then transferred to individual 50 mL plastic tubes and centrifuged for 15 min at 15 000g before the supernatant was carefully removed with a pipette. The SPAC pellets were dried at 40 °C for 48 h and homogenized with a porcelain mortar prior to the SANS measurements.

For SANS analysis, the samples were loaded into quartz cells with a flight path length of 1 mm (Hellma USA Inc., Plainview, NY, USA) on the General-Purpose SANS beamline (CG-2) at the Oak Ridge National Laboratory's high flux isotope reactor (HFIR).⁴⁵ Three configurations with $\lambda = 12$ Å with a wavelength spread, $\Delta \lambda/\lambda$, of 0.13 and a sample-to-detector distance (SDD) of 19.2 m and $\lambda = 4.75$ Å with $\Delta \lambda / \lambda = 0.13$ and SDDs of 6.8 and 1.0 m were used to cover the scattering vector Q range between 0.0015 and 0.7 Å⁻¹. All measurements were conducted under ambient conditions. The total scattering cross sections were calibrated using porous silica and corrected for empty cell scattering, sample transmission, thickness, and detector sensitivity. The azimuthally isotropic two-dimensional scattering patterns were then reduced to one-dimensional intensity I values as a function of Q. The data were analyzed with the polydisperse sphere (PDSP) model using PRINSAS, a software widely used to analyze the small-angle scattering (SAS) data of porous materials.^{46,47} In addition, the unified model for the analysis of SAS data from hierarchical materials was used (see the Supporting Information for additional details).48

Analytical Procedures. BPA was quantified using an Agilent 1200 Series HPLC system equipped with a diode array detector and a fluorescence detector (FLD) in serial configuration. 12 Separation was performed on an Agilent Eclipse XDB C18 column (4.6 mm \times 150 mm, 5 μ m) using isocratic elution at a flow rate of 1 mL min⁻¹ acetonitrile and Milli-Q water (50:50, v/v) at pH 7.2. The FLD was set at excitation and emission wavelengths of 226 and 310 nm, respectively. For standard curve preparation, vials containing 0.4, 1.1, 2.2, 11, 44, and 88 μ M BPA and 50 mg mL⁻¹ Lascorbic acid were prepared in triplicates (Figure S4). The limit of detection and the limit of quantification were 0.4 and 1.1 µM BPA with signal-to-noise ratios of 3:1 and 10:1, respectively.

RESULTS

BPA Degradation by Oxidized Mn Species. Batch experiments demonstrated BPA degradation with solid phase MnO₂, a finding corroborating prior reports. 12,13 degradation was also observed in incubation vessels with soluble Mn(III), indicating that both solid phase MnO2 and soluble Mn(III) degrade BPA (Figure 1). No BPA loss was observed in incubations lacking oxidized Mn species, indicating that the sorption of BPA to the experimental vessels was negligible (Figure 1).

The initial MnO₂ loading significantly affected the rate of BPA degradation, an effect that was less pronounced with Mn(III) as an oxidant (Figure 1 and Figure S5). The initial BPA concentration decreases followed pseudo-first order

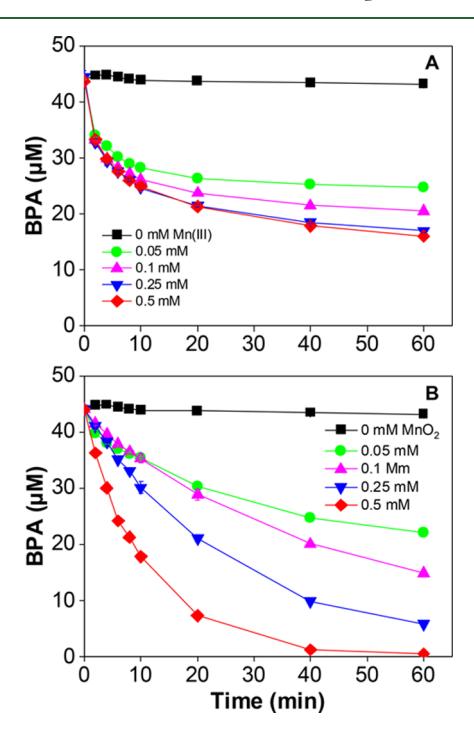


Figure 1. BPA concentration profiles in the presence of different concentrations of oxidized Mn species. (A) Mn(III)-mediated BPA degradation in incubation vessels with 5 mM phosphate buffer (pH 7.2) initially containing 44 μ M BPA over a 1 h incubation period. (B) α-MnO₂-mediated BPA degradation in incubation vessels with phosphate buffer (pH 7.2) initially containing 44 µM BPA. MnO₂ is expressed as nominal concentration. Error bars represent the standard deviation of duplicate samples and are not depicted when smaller than the symbol size.

reaction kinetics, but the rates decreased after about 8 min in both systems that received with MnO2 or Mn(III) (Figure 1). An initial BPA removal rate of 0.04 \pm 0.003 min⁻¹ was measured with 0.05 mM Mn(III), and a slightly higher rate of $0.05 \pm 0.002 \text{ min}^{-1}$ was observed with 0.5 mM Mn(III) (Figure S5A). While the initial degradation rate data suggested that BPA removal was not sensitive to the Mn(III) loading, the limited temporal resolution of the discontinuous analytical approach may have masked initial rate differences (Figure 1A). Over longer incubation periods, the amount of BPA removed was clearly Mn(III) loading-dependent (Figure S6). Increased MnO₂ loadings resulted in progressively higher initial BPA degradation rates (Figure 1B). In vessels with 0.05, 0.1, 0.25, and 0.5 mM MnO₂, BPA removal rates of 0.02 \pm 0.003, 0.03 \pm 0.001, 0.06 ± 0.004 , and $0.10 \pm 0.01 \text{ min}^{-1}$, respectively, were measured (Figure S5B). The maximum BPA degradation rate observed with MnO₂ was 2.0 \pm 0.03-fold faster than the maximum rate observed in vessels with soluble Mn(III) (Figure S5). Over a 1 h reaction period, $49.7 \pm 1.20\%$ of the initial 1.76 μ mol of BPA was removed with 0.05 mM MnO₂, and nearly complete removal (98.8 ± 0.01%) was achieved with 0.5 mM MnO₂. In contrast, approximately half (59%) of the initial 1.76 μ mol of BPA was degraded within 1 h in vessels with 0.5 mM Mn(III) (Figure 1A). To achieve the same BPA removal with Mn(III), longer incubation periods were required (e.g., 4 days in the presence of 0.5 mM Mn[III]) (Figure S6).

Adsorption Isotherms. The adsorption of BPA to SPAC reached equilibrium within 0.5 h, indicating that BPA sorption is a fast process. Analysis of the data showed that a Langmuir isotherm ($R^2 = 0.99$) fits the adsorption data slightly better than did the Freundlich isotherm ($R^2 = 0.96$) (Figure S7). Using the Langmuir model, a maximum adsorption capacity of 357 mg BPA per g of SPAC was determined. The amount of BPA that could be extracted with ethyl acetate gradually decreased as a function of time, whereas the fraction of nonextractable BPA increased (Figure S8). The aging process followed pseudo-first-order reaction kinetics and occurred at a rate of 5.54 ± 0.02 day⁻¹. Following a 60 day incubation, only $20.1 \pm 0.2\%$ of the initial 1.76 (± 0.02) μ mol of BPA adsorbed to SPAC could be extracted with ethyl acetate (Figure S8).

Degradation of BPA Adsorbed to SPAC. To explore if adsorbed BPA is susceptible to oxidative transformation, SPAC with adsorbed BPA was incubated with Mn(III) or MnO₂. Both Mn(III) and MnO₂ degraded dissolved BPA (Figure 1); however, only soluble Mn(III) degraded fresh and aged BPA adsorbed to SPAC (Figure 2). Following a 15 day incubation period, only about 11% of the initial 1.76 \pm 0.02 μ mol of freshly adsorbed BPA remained in incubations with 0.5 mM soluble Mn(III) (Figure 2B). In incubations with aged adsorbed BPA and 0.5 mM Mn(III), the initial 0.37 \pm 0.01 umol of solvent-extractable BPA was completely degraded during an 8 day incubation (Figure 2C). Degradation of adsorbed BPA followed pseudo-first-order reaction kinetics, and rates of 0.27 \pm 0.01 and 0.78 \pm 0.03 day⁻¹ were observed for freshly prepared and aged adsorbed BPA, respectively, in the presence of 0.5 mM soluble Mn(III). In contrast, no BPA degradation was observed with up to 2 mM MnO₂ (nominal concentrations) (Figure 2A). In control incubations without oxidized Mn species, no BPA was detected in the aqueous phase over a 15 day incubation period (Figure S9), indicating that no BPA desorption had occurred.

Addition of 0.05 and 0.1 mM Mn(III) into vessels with 44 μ M (1.76 μ mol) dissolved BPA caused removals of 59 \pm 1.7

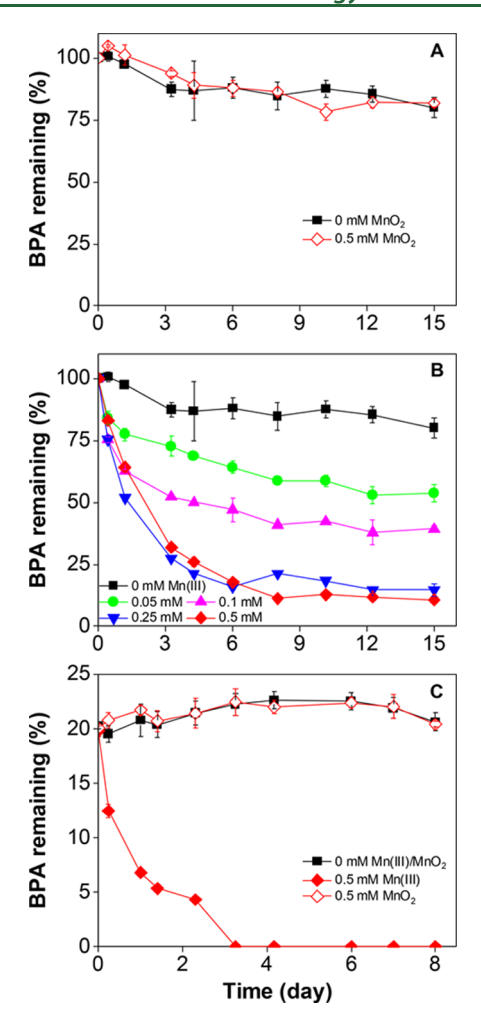


Figure 2. Degradation of BPA adsorbed to SPAC by oxidized Mn species. (A) Lack of removal of freshly adsorbed BPA in incubation vessels amended with solid α -MnO₂. BPA was incubated with SPAC for 30 min before the initiation of the experiments. (B) Soluble Mn(III)-mediated degradation of freshly adsorbed BPA. (C) Degradation of aged BPA adsorbed to SPAC by 0.5 mM soluble Mn(III) and 0.5 mM MnO2. BPA was incubated with SPAC for 60 days before initiation of the experiment. Experiments were performed using 1.44 mg of SPAC with 401 μ g of adsorbed BPA. The amount of BPA remaining was determined by HPLC following ethyl acetate extraction of suspension samples. α -MnO₂ is a solid and indicated are the nominal concentrations. Error bars represent the standard deviations of triplicate vessels and are not depicted when smaller than the symbol size.

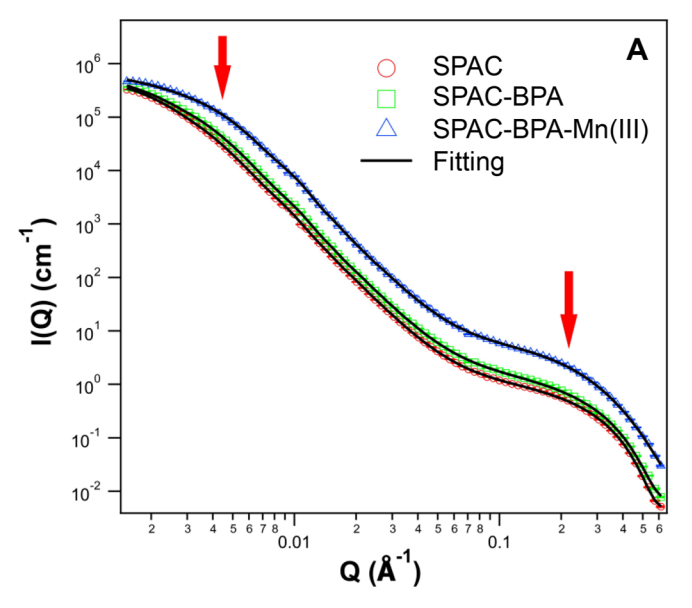
and 86 \pm 0.6% of BPA, respectively, after 4 days. Complete (100%) removal was observed with 0.25 and 0.5 mM Mn(III) (Figure S6). In vessels with the same amount of BPA freshly adsorbed to SPAC and the same Mn(III) concentrations, smaller amounts of BPA, ranging from 9.1 to 88.8%, were removed over the same period (Figure 2B). Apparently, Mn(III) degraded adsorbed BPA at lower rates than dissolved BPA, indicating that adsorption affects the rate and extent of BPA degradation.

Changes in Pore Size Due to BPA Adsorption and Degradation. To develop an understanding of BPA adsorption and degradation within the SPAC pore structure, SANS analysis was performed and the data were analyzed with the PDSP model. Figure 3A shows the SANS curves in the log-log space where I(Q) is the scattering intensity, and Q is

the scattering vector related to the neutron wavelength (λ) and the scattering angle (θ) as $Q = \left(\frac{4\pi}{\lambda}\right) \sin\left(\frac{\theta}{2}\right)$, which is a restatement of Bragg's law. 49 Nanoporous materials often exhibit hierarchical structures, which are reflected in these data by the two Guinier "knees" indicated by the arrows on the SANS curves in Figure 3A. These knees result from separate distributions of scatterers (pores in this case) with similar sizes, and their locations correlate with the radii of gyration (R_g) of the size limits of those distributions where $R_g \sim 2\pi/Q$. So, $R_g \sim 2\pi/Q$. was used to represent the pore size because the pores of SPAC have irregular and tortuous shapes. The volume-weighted pore size distributions (Figure 3B) indicate the presence of two major populations of pores in all three samples (Figure 3A). One is represented by micropores with an average size of ~8 Å and a noticeable shoulder at \sim 13 Å. The other population exhibits a broad size range from 100 to 900 Å in diameter (i.e., macropores). Adsorption of BPA caused little change to the micropore population other than a slight increase in the intensity of the ~13 Å shoulder (green line in Figure 3B and Figure S10). In contrast, the average size of the macropores decreased, suggesting that the BPA molecules adsorbed on the internal walls of these larger pores and formed a surface layer. As a result, the pores became smaller, an effect that was measurable with SANS because the SLD of deuterated BPA is close to that of activated carbon (green line in Figure 3B and Figure S10). Addition of soluble Mn(III) shifted the position of the main micropore peak from 8 to 7 Å, and its intensity decreased (blue line in Figure 3B). This shift was attributed to the migration of smaller BPA transformation products into the micropores. The shoulder also shifted from 13 to 11 Å, and its intensity increased significantly, presumably also a result of the penetration of BPA transformation products into micropores or due to a layer of BPA (approximately 11 Å in size) on the surface of the macropores. The SANS analysis further suggested that the average size of the larger pore population (level 2) decreased following Mn(III) treatment (blue line in Figure 3B and Figure S10).

Results obtained using the unified fit model, which was developed for modeling hierarchical materials, 48 support these conclusions. In this model, each structural level is defined by an equation with two parts: with a Guinier section defining a maximum intensity (G) and R_g defining the upper size limit of the level (see the Supporting Information for details), below which (e.g., at higher Q) the intensity of the Guinier section of the curve drops off rapidly.⁵² The rapid drop in intensity corresponds to the position of the knees mentioned above. A structurally limited power-law term contains a prefactor B governing its intensity and a power-law slope P related to surface roughness as well as the same R_g used in the Guinier section. This power-law term defines the slope and intensity at Q values above each knee. The prefactor B is often defined in terms of G, R_g , and P and thus is not an independent variable.

Based on the observation of two knees in the log-log scattering plots (Figure 3 and Figure S11), the SPAC appears to consist of two structural levels (i = 2) within the size range analyzed by SANS. Level 1 corresponds to the micropores, and level 2 corresponds to the population of pores ranging from 100 to 900 Å (Figure 3B). The scattering contributions from the different structural levels are decomposed in Figure S11, and the parameters obtained through the model fitting are shown in Table S2. The average $R_{\rm g}$ values for the macropores and micropores are 728.1 ± 0.3 and 7.9 ± 0.1 Å, respectively



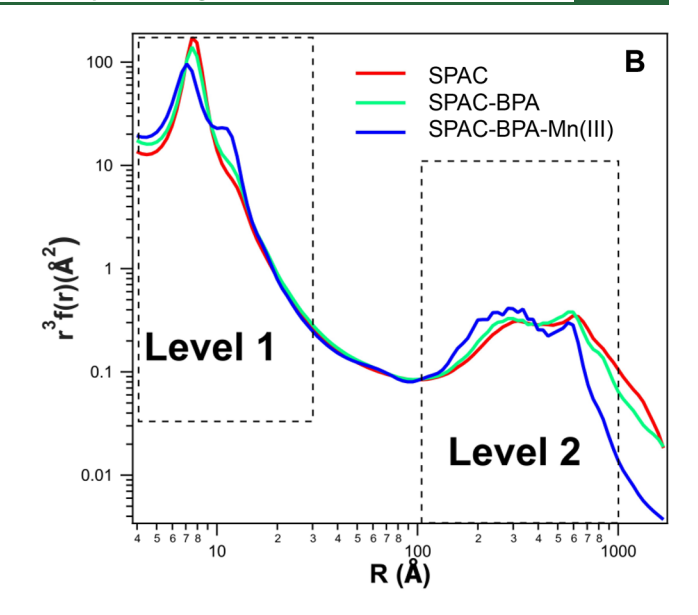


Figure 3. SANS profiles and data modeling. Panel (A) shows the background-subtracted SANS profiles for dried SPAC, dried SPAC with adsorbed deuterated BPA, and dried SPAC with adsorbed deuterated BPA after Mn(III)-mediated degradation. The solid black lines represent the best fit based on the PDSP model (see the Supporting Information for details). The arrows indicate the locations of knees where the slopes of the scattering curves change significantly. Panel (B) illustrates the volume-weighted f(r) distributions of three samples obtained from the PDSP model. f(r) represents the probability density of the pore size distribution, which is defined as the number of pores within an interval between r and r + dr normalized to the total number of pores. A two-level unified model was also applied to fit SANS data, and the results are shown in Table 1 and Figure S11.

(Table 1). Upon sorption of deuterated BPA, the size of the macropores decreased by \sim 10%, indicating adsorption of BPA

Table 1. Radii of Pore Structure Levels of SPAC, SPAC with Adsorbed Deuterated BPA, and SPAC after Mn(III)-Mediated Degradation of Adsorbed Deuterated BPA

	$R_{ m g}$ (Å)		
structure level	SPAC	SPAC-BPA	SPAC-BPA-Mn(III)
level 1	7.9 ± 0.1	8.5 ± 0.1	8.9 ± 0.1
level 2	728.1 ± 0.3	653.8 ± 0.2	494.2 ± 0.1

(Figure S10). A 6% size increase in the micropores (level 1 structure) was also observed, which presumably reflects the adsorption of 11 Å BPA molecules in the macropores, ⁵³ an interpretation supported by the PDSP fitting results.

After the addition of soluble Mn(III), the larger pores experienced a further reduction in average size by \sim 24%, while the $R_{\rm g}$ values for the micropores showed a measurable increase of 4%. These observations suggest migration of BPA transformation products into the micropores as well as a continuation of the processes adding an adsorbed layer to the macropores. Overall, the SANS data provide direct evidence for adsorption of transformation products of deuterated BPA throughout the SPAC pore structure.

DISCUSSION

Sediments are major sinks for and reservoirs of BPA in the environment, and an understanding of the processes that affect the fate and the longevity of BPA is relevant to predicting potential human exposure. MnO₂ is a reactive phase with a high oxidation potential capable of oxidizing various types of organic and inorganic compounds, including BPA. 12,54,55 A primary source of natural MnO₂ minerals is microbial oxidation of Mn(II), a process that can occur under both

oxic^{56,57} and anoxic^{58,59} conditions. MnO₂ polymorphs occur commonly in natural sediments, and 26–348 mg L⁻¹ MnO₂ has been reported in freshwater sediments^{60,61} and 2–16 mg L⁻¹ in the surface layer of marine sediments.⁶² In addition to Mn(IV), Mn(III) is a strong oxidant, which has been recognized to play a role in biogeochemical cycling,^{63–66} and is an intermediate in biotic Mn(II) oxidation,⁶⁷ biotic MnO₂ reduction,²² and abiotic permanganate reduction.⁶⁸ Free aqueous Mn(III) is short-lived and undergoes disproportionation to soluble Mn(II) and solid Mn(IV)²¹ but commonly occurs in environmental systems such as soils,⁶⁵ natural water bodies,²⁶ and sediments.²⁵ This is due to the formation of stable, water-soluble Mn(III) complexes with natural ligands, including pyrophosphate,²⁷ oxalate,⁶⁴ citrate,⁶⁹ and siderophores.²¹

BPA Degradation by Oxidized Mn Species. The experimental efforts reported here have demonstrated that, in addition to MnO2, Mn(III) mediates BPA degradation. Reactivity with BPA was observed at Mn(III) and MnO₂ (nominal) concentrations as low as 50 μ M. Mn concentrations in this range have been reported in various environmental settings, $^{60-62}$ suggesting that BPA degradation by oxidized Mn can occur in situ, and Mn-mediated oxidation may be a relevant natural attenuation process.^{9,12} The BPA degradation rates in experimental vessels with Mn(III) decreased over time (Figure 1A), similar to what was observed in MnO₂-bearing systems (Figure 1B). 12,13 The highest BPA degradation rates with Mn(III) were observed during the initial reaction phase and were largely independent of the initial Mn(III) loading (Figure 1A and Figure S5) but then decreased within minutes (Figure 1A). A possible explanation for the decreasing rates over time is the formation of transformation products, such as 4hydroxycumyl alcohol (HCA), which are also susceptible to oxidation by Mn(III). Further, Mn(II) may affect the reactivity of Mn(III), and passivation of solid MnO₂ by Mn(II) has been described. 12,70

Adsorption of BPA to Activated Carbon (SPAC) **Nanopores.** With a $\log_{K_{OW}}$ of 3.42,²⁹ an aqueous solubility of 300 mg L⁻¹ at 25 °C, ⁷¹ and Henry's law constant of 1.0 \times 10⁻¹⁰ atm m³ mol⁻¹, ¹ BPA is not volatile at ambient temperature and has a tendency to adsorb on hydrophobic surfaces. In our experiments, BPA sorption to SPAC reached the capacity expected for carbon-based porous materials (Figure S7), 32,72 and SANS analysis confirmed the adsorption of BPA within the macropores of the SPAC pore structure. BPA adsorption could be described by a Langmuir isotherm indicative of monolayer adsorption.⁷³ A decrease in organic solvent extractable BPA was observed with increasing incubation time (i.e., aging) (Figure S8), suggesting that BPA adsorption changed from physisorption based on van der Waals forces to chemisorption. In support of this hypothesis, prolonged extraction periods (e.g., 3 days) to recover more sorbed BPA were not successful. A previous study demonstrated increases in macropore and micropore porosity following organic solvent extraction,⁷⁴ suggesting that the extraction solvent can reach BPA adsorbed in the SPAC macropores. Most likely, the formation of bound residues (i.e., covalent bond formation between SPAC and BPA) limited extractability of aged BPA adsorbed to SPAC, a phenomenon that has been described for a variety of organic compounds, including BPA and tetrabromobisphenol A, adsorbed to solid matrices.7

SANS Analysis of Mn(III)-Treated SPAC. Treatment with Mn(III) decreased the amount of extractable BPA, and SANS analysis revealed that this process was coupled with changes to the sizes of macro- and micropores of SPAC. The observed pore size changes suggest that adsorbed BPA degradation mainly occurred in the larger SPAC pores in the 100-900 Å size range. BPA has a molecular size of ~11 Å, 77 which makes it physically impossible for BPA molecules to penetrate the SPAC micropores. Degradation of BPA molecules led to a shift of the shoulder peak from 13 to 11 Å and increased its volume fraction (Figure 3B). In addition, the intensity of the smaller micropore peak decreased and shifted from 8 to 7 Å. The latter is presumably due to the formation of BPA transformation products of smaller molecular size (e.g., HCA, 4-isopropenylphenol)^{12,78} that can diffuse out of the larger pores and migrate into the micropores (Figure S10). The 4% increase in the average size of level 1 structures obtained with the unified modeling method was attributed to the significant increase in the volume fraction of the shoulder peak (Figure 3B).

The SANS analysis also suggested a decrease in the size of the larger pores following Mn(III) treatment. This shift of the average macropore size (indicated by the blue line in Figure 3B) is much larger than the size of a single BPA molecule, suggesting the formation of molecules that are larger than BPA (e.g., BPA dimers) in response to the Mn(III) treatment. 13,78 The macropores also provide diffusion channels for Mn(III), and thus, a pore size reduction may hinder the deeper penetration of soluble Mn(III) into the SPAC, a possible explanation for the observed incomplete degradation of adsorbed BPA (Figure 2).

The discussion above presents a sensible interpretation of the SANS data focused on the changes in pore size of SPAC caused by BPA and its transformation products; however, a few uncertainties should be considered. For example, the reduction of Mn(III) leads to the formation of Mn(II), and adsorption to

different types of activated carbon has been demonstrated.^{79,80} The SPAC used in our experiments was loaded with adsorbed BPA, and the BPA transformation products formed following Mn(III) treatment also adsorb to SPAC, possibly limiting the adsorption sites for Mn(II). 75,76 Further, the Mn(II) ion is much smaller than a BPA molecule, 77 and it is unlikely that Mn(II) adsorption affected the experimental results. Another potential issue is the formation of Mn(II) phosphate (i.e., Mn₃[PO₄]₂) precipitate. We never observed precipitate formation presumably because the reaction conditions were not conducive for precipitate formation, 81 and interference by Mn₃(PO₄)₂ precipitate is unlikely. Pyrophosphate was present in all experiments and was therefore not a variable, indicating that the adsorption of pyrophosphate was not a factor complicating the interpretation of the SANS data. Further, it is theoretically possible that Mn(III) oxidizes SPAC, causes dissolution, and alters the pore size structure; however, experimental evidence for such processes is lacking.

Degradation of dissolved BPA by MnO2 is an established process; 12,13 however, our results demonstrated that the α -MnO₂ particles used in our experiments could not mediate degradation of BPA adsorbed to activated carbon (i.e., SPAC). The α -MnO₂ particle size exceeded that of a SPAC particle by more than 10-fold (i.e., 15.41 \pm 1.35 versus 1.38 \pm 0.03 μ m, respectively) and was much larger than the pores of the SPAC particles. The experimental data indicated strong adsorption of BPA to SPAC as no BPA was released over time. As a result, physical separation prevented oxidation of BPA by solid-phase MnO₂. In contrast, soluble Mn(III), which could enter the pore structure of the SPAC, mediated the degradation of adsorbed BPA. Generally, desorption of hydrophobic compounds and their diffusion out of the pore structure are thought to be required steps for degradation; ^{32,34,35} however, the findings reported here indicate that the diffusion of BPA out of the SPAC pore structure was not required for degradation to occur. It remains to be determined if Mn(III) directly interacts with adsorbed BPA or if desorption within the pore structure is required for oxidative attack within the

Environmental Implications. Adsorbed BPA occurs in a number of environmental systems and has been reported in soils $(0.5-325 \text{ ng BPA g}^{-1}, \text{dry weight})$, sediments (1.49-13)370 ng BPA g⁻¹, dry weight), and sewage sludge (4–1363 ng BPA L⁻¹, dry weight), which are considered major sinks and reservoirs for BPA. Although these materials have unique physicochemical properties that distinguish them from SPAC,^{35,82} they often possess broadly similar hydrophobic pore structures in the nanometer to micrometer size range. 82,83 Mn(III) also occurs in various environmental systems, and the finding that Mn(III) contributes to BPA degradation, including the degradation of adsorbed BPA, advances our understanding of natural attenuation processes that affect the fate and longevity of BPA as well as other hydrophobic compounds susceptible to Mn(III) degradation. By extension, these findings also suggest a possible method for treating BPAcontaminated environments. Areas with elevated Mn(III) concentrations and active Mn cycling, such as oxic-anoxic transition zones are, therefore, likely hotspot zones for oxidized Mn-mediated BPA degradation. Such transition zones may function as natural barriers controlling the release of BPA to the overlying water column, minimizing human exposure risk. The new findings can inform models that more accurately predict BPA behavior in sediments and soils and generate

opportunities for engineering solutions aimed at reducing BPA release to surface waters, thereby mitigating human health concerns.

ASSOCIATED CONTENT

Supporting Information

The Supporting Information is available free of charge at https://pubs.acs.org/doi/10.1021/acs.est.1c03862.

MnO₂ quantification, characterization, and particle size analysis; Table S1: particle size distribution of SPAC and MnO₂; Table S2: modeling parameters of SANS profiles; Figure S1: UV spectra of soluble Mn(III) and BPA; Figure S2: standard curve to determine nominal MnO₂ concentrations; Figure S3: XRD pattern of MnO₂ synthesized in the present study; Figure S4: representative standard curve for determining BPA concentrations; Figure S5: effect of soluble Mn(III) and MnO₂ loadings on BPA degradation rate constants; Figure S6: Mn(III)mediated BPA degradation in incubation vessels with phosphate buffer (pH 7.2); Figure S7: adsorption characteristics of BPA to SPAC in systems without Mn; Figure S8: recovery of BPA from SPAC following solvent extraction as a function of time; Figure S9: desorption kinetics of BPA from SPAC at pH 6, 7.2, and 8.2; Figure S10: schematic illustration of micropores (level 1) and a macropore (level 2) within an activated carbon SPAC particle; and Figure S11: decomposition of total SANS scattering of SPAC, SPAC-BPA, and SPAC-BPA-Mn(III) into scattering from incoherent scattering background and pores with different sizes (PDF)

AUTHOR INFORMATION

Corresponding Author

Frank E. Löffler - Department of Civil and Environmental Engineering, Center for Environmental Biotechnology, Department of Microbiology, and Department of Biosystems Engineering and Soil Science, University of Tennessee, Knoxville, Tennessee 37996, United States; Biosciences Division, Oak Ridge National Laboratory, Oak Ridge, Tennessee 37831, United States; o orcid.org/0000-0002-9797-4279; Phone: (865) 974-4933; Email: frank.loeffler@utk.edu

Authors

Yanchen Sun – Department of Civil and Environmental Engineering and Center for Environmental Biotechnology, University of Tennessee, Knoxville, Tennessee 37996, United States; Biosciences Division, Oak Ridge National Laboratory, Oak Ridge, Tennessee 37831, United States; oorcid.org/ 0000-0003-1265-2738

Jeongdae Im - Department of Civil Engineering, Kansas State University, Manhattan, Kansas 66503, United States; orcid.org/0000-0002-6871-5366

Nusrat Shobnam - Department of Civil Engineering, Kansas State University, Manhattan, Kansas 66503, United States Sofia K. Fanourakis - Department of Materials Science and Engineering, University of Houston, Houston, Texas 77204, United States

Lilin He - Neutron Scattering Division, Oak Ridge National Laboratory, Oak Ridge, Tennessee 37831, United States

Lawrence M. Anovitz - Chemical Sciences Division, Oak Ridge National Laboratory, Oak Ridge, Tennessee 37831, United States; orcid.org/0000-0002-2609-8750

Paul R. Erickson - REGENESIS, San Clemente, California 92673, United States

Huihui Sun – Department of Biosystems Engineering and Soil Science, University of Tennessee, Knoxville, Tennessee 37996,

Jie Zhuang - Department of Biosystems Engineering and Soil Science, University of Tennessee, Knoxville, Tennessee 37996, United States; orcid.org/0000-0002-5472-9118

Complete contact information is available at: https://pubs.acs.org/10.1021/acs.est.1c03862

Notes

The authors declare no competing financial interest.

ACKNOWLEDGMENTS

This work was supported by the Polycarbonate/BPA Global Group of the American Chemistry Council (ACC), Washington, DC. A portion of this research used resources at the High Flux Isotope Reactor, a DOE Office of Science User Facility operated by the Oak Ridge National Laboratory. Effort by L.M.A. was supported by research sponsored by the Division of Chemical Sciences, Geosciences, and Biosciences, Office of Basic Energy Sciences, U.S. Department of Energy. Y.S. acknowledges the support from the China Scholarship Council.

REFERENCES

- (1) Staples, C. A.; Dome, P. B.; Klecka, G. M.; Oblock, S. T.; Harris, L. R. A review of the environmental fate, effects, and exposures of bisphenol A. Chemosphere 1998, 36, 2149-2173.
- (2) Experts, I. Bisphenol-A A Global Market Overview. 2016, Report Code: CP021, https://industry-experts.com/verticals/files/articles/ cp021-bisphenol-a-a-global-market-overview.pdf (accessed May 10, 2020).
- (3) Huang, D.-Y.; Zhao, H.-Q.; Liu, C.-P.; Sun, C.-X. Characteristics, sources, and transport of tetrabromobisphenol A and bisphenol A in soils from a typical e-waste recycling area in South China. Environ. Sci. Pollut. Res. 2014, 21, 5818-5826.
- (4) Liao, C.; Liu, F.; Moon, H.-B.; Yamashita, N.; Yun, S.; Kannan, K. Bisphenol analogues in sediments from industrialized areas in the United States, Japan, and Korea: spatial and temporal distributions. Environ. Sci. Technol. 2012, 46, 11558-11565.
- (5) Liao, C.; Liu, F.; Guo, Y.; Moon, H.-B.; Nakata, H.; Wu, Q.; Kannan, K. Occurrence of eight bisphenol analogues in indoor dust from the United States and several Asian countries: implications for human exposure. Environ. Sci. Technol. 2012, 46, 9138-9145.
- (6) Fromme, H.; Küchler, T.; Otto, T.; Pilz, K.; Müller, J.; Wenzel, A. Occurrence of phthalates and bisphenol A and F in the environment. Water Res. 2002, 36, 1429-1438.
- (7) Kinch, C. D.; Ibhazehiebo, K.; Jeong, J.-H.; Habibi, H. R.; Kurrasch, D. M. Low-dose exposure to bisphenol A and replacement bisphenol S induces precocious hypothalamic neurogenesis in embryonic zebrafish. Proc. Natl. Acad. Sci. U. S. A. 2015, 112, 1475-1480.
- (8) Hernandez, M. E.; Gore, A. C. Endocrine disruptors: Chemical contaminants—A toxic mixture for neurodevelopment. Nat. Rev. Endocrinol. 2017, 13, 322.
- (9) Im, J.; Löffler, F. E. Fate of bisphenol A in terrestrial and aquatic environments. Environ. Sci. Technol. 2016, 50, 8403-8416.
- (10) Chen, Y.; Stemple, B.; Kumar, M.; Wei, N. Cell surface display fungal laccase as a renewable biocatalyst for degradation of persistent

- micropollutants bisphenol A and sulfamethoxazole. *Environ. Sci. Technol.* **2016**, *50*, 8799–8808.
- (11) Eio, E. J.; Kawai, M.; Niwa, C.; Ito, M.; Yamamoto, S.; Toda, T. Biodegradation of bisphenol A by an algal-bacterial system. *Environ. Sci. Pollut. Res.* **2015**, 22, 15145–15153.
- (12) Im, J.; Prevatte, C. W.; Campagna, S. R.; Löffler, F. E. Identification of 4-hydroxycumyl alcohol as the major MnO₂-mediated bisphenol A transformation product and evaluation of its environmental fate. *Environ. Sci. Technol.* **2015**, *49*, 6214–6221.
- (13) Lin, K.; Liu, W.; Gan, J. Oxidative removal of bisphenol A by manganese dioxide: efficacy, products, and pathways. *Environ. Sci. Technol.* **2009**, 43, 3860–3864.
- (14) Ju, L.; Wu, P.; Yang, Q.; Ahmed, Z.; Zhu, N. Synthesis of ZnAlTi-LDO supported C60@ AgCl nanoparticles and their photocatalytic activity for photo-degradation of bisphenol A. *Appl. Catal., B.* **2018**, 224, 159–174.
- (15) Zhang, Y.; Tang, Y.; Qin, Z.; Luo, P.; Ma, Z.; Tan, M.; Kang, H.; Huang, Z. A novel manganese oxidizing bacterium-Aeromonas hydrophila strain DS02: Mn (II) oxidization and biogenic Mn oxides generation. *J. Hazard. Mater.* **2019**, *367*, 539–545.
- (16) Sigel, H. Manganese in natural waters and earth's crust: Its availability to organisms. In *Metal Ions in Biological Systems*; CRC Press, 2000; pp 49–82.
- (17) Post, J. E. Manganese oxide minerals: Crystal structures and economic and environmental significance. *Proc. Natl. Acad. Sci. U. S. A.* 1999, 96, 3447–3454.
- (18) Burdige, D. J. The biogeochemistry of manganese and iron reduction in marine sediments. *Earth-Sci. Rev.* **1993**, *35*, 249–284.
- (19) Chen, G.; Zhao, L.; Dong, Y.-h. Oxidative degradation kinetics and products of chlortetracycline by manganese dioxide. *J. Hazard. Mater.* **2011**, 193, 128–138.
- (20) Stone, A. T. Reductive dissolution of manganese (III/IV) oxides by substituted phenols. *Environ. Sci. Technol.* **1987**, 21, 979–988
- (21) Webb, S. M.; Dick, G. J.; Bargar, J. R.; Tebo, B. M. Evidence for the presence of Mn (III) intermediates in the bacterial oxidation of Mn (II). *Proc. Natl. Acad. Sci. U. S. A.* **2005**, 102, 5558–5563.
- (22) Lin, H.; Szeinbaum, N. H.; DiChristina, T. J.; Taillefert, M. Microbial Mn (IV) reduction requires an initial one-electron reductive solubilization step. *Geochim. Cosmochim. Acta* **2012**, 99, 179–192.
- (23) Liu, W.; Sun, B.; Qiao, J.; Guan, X. Influence of pyrophosphate on the generation of soluble Mn (III) from reactions involving Mn oxides and Mn (VII). *Environ. Sci. Technol.* **2019**, *53*, 10227–10235.
- (24) Johnson, K. S. Manganese redox chemistry revisited. *Science* **2006**, 313, 1896–1897.
- (25) Madison, A. S.; Tebo, B. M.; Mucci, A.; Sundby, B.; Luther, G. W., III Abundant porewater Mn (III) is a major component of the sedimentary redox system. *Science* **2013**, *341*, 875–878.
- (26) Trouwborst, R. E.; Clement, B. G.; Tebo, B. M.; Glazer, B. T.; Luther, G. W., III Soluble Mn (III) in suboxic zones. *Science* **2006**, 313, 1955–1957.
- (27) Kostka, J. E.; Luther, G. W., III; Nealson, K. H. Chemical and biological reduction of Mn (III)-pyrophosphate complexes: potential importance of dissolved Mn (III) as an environmental oxidant. *Geochim. Cosmochim. Acta* 1995, 59, 885–894.
- (28) Hu, E.; Zhang, Y.; Wu, S.; Wu, J.; Liang, L.; He, F. Role of dissolved Mn (III) in transformation of organic contaminants: non-oxidative versus oxidative mechanisms. *Water Res.* **2017**, *111*, 234–243.
- (29) Borrirukwisitsak, S.; Keenan, H. E.; Gauchotte-Lindsay, C. Effects of salinity, pH and temperature on the octanol-water partition coefficient of bisphenol A. *Int. J. Environ. Sci. Technol.* **2012**, *3*, 460.
- (30) Li, J.; Zhou, B.; Liu, Y.; Yang, Q.; Cai, W. Influence of the coexisting contaminants on bisphenol A sorption and desorption in soil. *J. Hazard. Mater.* **2008**, *151*, 389–393.
- (31) Fei, Y.-H.; Leung, K. M. Y.; Li, X.-y. Adsorption and desorption behaviors of selected endocrine disrupting chemicals in simulated gastrointestinal fluids. *Mar. Pollut. Bull.* **2014**, *85*, 363–369.

- (32) Kim, J. R.; Huling, S. G.; Kan, E. Effects of temperature on adsorption and oxidative degradation of bisphenol A in an acid-treated iron-amended granular activated carbon. *Chem. Eng. J.* **2015**, 262, 1260–1267.
- (33) Bele, S.; Samanidou, V.; Deliyanni, E. Effect of the reduction degree of graphene oxide on the adsorption of bisphenol A. *Chem. Eng. Res. Des.* **2016**, *109*, 573–585.
- (34) Kan, E.; Huling, S. G. Effects of temperature and acidic pretreatment on fenton-driven oxidation of MTBE-spent granular activated carbon. *Environ. Sci. Technol.* **2009**, 43, 1493–1499.
- (35) Fan, D.; Gilbert, E. J.; Fox, T. Current state of in situ subsurface remediation by activated carbon-based amendments. *J. Environ. Manage.* **2017**, 204, 793–803.
- (36) Zhang, R.; Liu, S.; Bahadur, J.; Elsworth, D.; Melnichenko, Y.; He, L.; Wang, Y. Estimation and modeling of coal pore accessibility using small angle neutron scattering. *Fuel* **2015**, *161*, 323–332.
- (37) Anovitz, L. M.; Cole, D. R. Characterization and analysis of porosity and pore structures. *Rev. Mineral. Geochem.* **2015**, *80*, 61–164
- (38) Kostka, J.; Nealson, K. H. Isolation, cultivation and characterization of iron-and manganese-reducing bacteria. In *Techniques in Microbial Ecology*; Oxford University Press, 1998; pp. 58–78.
- (39) Sun, B.; Guan, X.; Fang, J.; Tratnyek, P. G. Activation of manganese oxidants with bisulfite for enhanced oxidation of organic contaminants: the involvement of Mn (III). *Environ. Sci. Technol.* **2015**, *49*, 12414–12421.
- (40) Krumbein, W. E.; Altmann, H. J. A new method for the detection and enumeration of manganese oxidizing and reducing microorganisms. *Helgoländer Wissenschaftliche Meeresuntersuchungen* 1973, 25, 347.
- (41) Limousin, G.; Gaudet, J.-P.; Charlet, L.; Szenknect, S.; Barthès, V.; Krimissa, M. Sorption isotherms: A review on physical bases, modeling and measurement. *Appl. Geochem.* **2007**, *22*, 249–275.
- (42) Figueroa, R. A.; MacKay, A. A. Sorption of oxytetracycline to iron oxides and iron oxide-rich soils. *Environ. Sci. Technol.* **2005**, 39, 6664–6671.
- (43) Im, J.; Prevatte, C. W.; Lee, H. G.; Campagna, S. R.; Löffler, F. E. 4-Methylphenol produced in freshwater sediment microcosms is not a bisphenol A metabolite. *Chemosphere* **2014**, *117*, 521–526.
- (44) Xu, J.; Wu, L.; Chen, W.; Chang, A. C. Simultaneous determination of pharmaceuticals, endocrine disrupting compounds and hormone in soils by gas chromatography—mass spectrometry. *J. Chromatogr. A* **2008**, *1202*, 189–195.
- (45) Heller, W. T.; Cuneo, M.; Debeer-Schmitt, L.; Do, C.; He, L.; Heroux, L.; Littrell, K.; Pingali, S. V.; Qian, S.; Stanley, C.; Urban, V. S.; Wu, B.; Bras, W. The suite of small-angle neutron scattering instruments at Oak Ridge National Laboratory. *J. Appl. Crystallogr.* **2018**, *51*, 242–248.
- (46) Hinde, A. L. PRINSAS—a Windows-based computer program for the processing and interpretation of small-angle scattering data tailored to the analysis of sedimentary rocks. *J. Appl. Crystallogr.* **2004**, 37, 1020—1024.
- (47) Ilavsky, J.; Jemian, P. R. Irena: tool suite for modeling and analysis of small-angle scattering. *J. Appl. Crystallogr.* **2009**, *42*, 347–353.
- (48) Beaucage, G. Approximations leading to a unified exponential/power-law approach to small-angle scattering. *J. Appl. Crystallogr.* **1995**, 28, 717–728.
- (49) Bragg, W. H.; Bragg, W. L. The reflection of X-rays by crystals. *Proc. R. Soc. London, Ser. A* 1913, 88, 428–438.
- (50) Krzysko, A. J.; Nakouzi, E.; Zhang, X.; Graham, T. R.; Rosso, K. M.; Schenter, G. K.; Ilavsky, J.; Kuzmenko, I.; Frith, M. G.; Ivory, C. F.; Clark, S. B.; Weston, J. S.; Weigandt, K. M.; de Yoreo, J. J.; Chun, J.; Anovitz, L. M. Correlating inter-particle forces and particle shape to shear-induced aggregation/fragmentation and rheology for dilute anisotropic particle suspensions: A complementary study via capillary rheometry and in-situ small and ultra-small angle X-ray scattering. *J. Colloid Interface Sci.* 2020, 576, 47–58.

- (51) Weston, J. S.; Chun, J.; Schenter, G.; Weigandt, K.; Zong, M.; Zhang, X.; Rosso, K. M.; Anovitz, L. M. Connecting particle interactions to agglomerate morphology and rheology of boehmite nanocrystal suspensions. *J. Colloid Interface Sci.* **2020**, *572*, 328–339.
- (52) Guinier, A.; Fournet, G.; Yudowitch, K. L. Small-angle scattering of X-rays; John Wiley & Sons Press, 1955.
- (53) Wei, Y.; Hore, M. J. A. Characterizing polymer structure with small-angle neutron scattering: A Tutorial. *J. Appl. Phys.* **2021**, *129*, 171101.
- (54) Beal, E. J.; House, C. H.; Orphan, V. J. Manganese- and iron-dependent marine methane oxidation. *Science* **2009**, 325, 184–187.
- (55) Nico, P. S.; Zasoski, R. J. Mn (III) center availability as a rate controlling factor in the oxidation of phenol and sulfide on δ -MnO₂. *Environ. Sci. Technol.* **2001**, *35*, 3338–3343.
- (56) Hansel, C. M. Manganese in marine microbiology. In *Advances in microbial physiology*; Elsevier, 2017; Vol. 70, pp. 37–83.
- (57) Shobnam, N.; Sun, Y.; Mahmood, M.; Löffler, F. E.; Im, J. Biologically mediated abiotic degradation (BMAD) of bisphenol A by manganese-oxidizing bacteria. *J. Hazard. Mater.* **2021**, 125987.
- (58) Daye, M.; Klepac-Ceraj, V.; Pajusalu, M.; Rowland, S.; Farrell-Sherman, A.; Beukes, N.; Tamura, N.; Fournier, G.; Bosak, T. Light-driven anaerobic microbial oxidation of manganese. *Nature* **2019**, *576*, 311–314.
- (59) Yu, H.; Leadbetter, J. R. Bacterial chemolithoautotrophy via manganese oxidation. *Nature* **2020**, *583*, 453–458.
- (60) Kepkay, P. E. Kinetics of microbial manganese oxidation and trace metal binding in sediments: Results from an in situ dialysis technique. *Limnol. Oceanogr.* **1985**, *30*, 713–726.
- (61) Sigg, L.; Sturm, M.; Kistler, D. Vertical transport of heavy metals by settling particles in Lake Zurich. *Limnol. Oceanogr.* **1987**, 32, 112–130.
- (62) Vandieken, V.; Pester, M.; Finke, N.; Hyun, J.-H.; Friedrich, M. W.; Loy, A.; Thamdrup, B. Three manganese oxide-rich marine sediments harbor similar communities of acetate-oxidizing manganese-reducing bacteria. *ISME J.* **2012**, *6*, 2078–2090.
- (63) Wang, Z.; Xiong, W.; Tebo, B. M.; Giammar, D. E. Oxidative UO₂ dissolution induced by soluble Mn (III). *Environ. Sci. Technol.* **2014**, *48*, 289–298.
- (64) Chen, W.-R.; Liu, C.; Boyd, S. A.; Teppen, B. J.; Li, H. Reduction of carbadox mediated by reaction of Mn (III) with oxalic acid. *Environ. Sci. Technol.* **2013**, *47*, 1357–1364.
- (65) Jones, M. E.; Nico, P. S.; Ying, S.; Regier, T.; Thieme, J.; Keiluweit, M. Manganese-driven carbon oxidation at oxic—anoxic interfaces. *Environ. Sci. Technol.* **2018**, *52*, 12349—12357.
- (66) Wesolowski, D. J.; Ziemniak, S. E.; Anovitz, L. M.; Machesky, M. L.; Bénézeth, P.; Palmer, D. A. Solubility and surface adsorption characteristics of metal oxides. In *Aqueous Systems at Elevated Temperatures and Pressures*; Elsevier, 2004, pp. 493–595.
- (67) Glenn, J. K.; Gold, M. H. Purification and characterization of an extracellular Mn (II)-dependent peroxidase from the lignin-degrading basidiomycete, Phanerochaete chrysosporium. *Arch. Biochem. Biophys.* **1985**, 242, 329–341.
- (68) Adler, S. J.; Noyes, R. M. The mechanism of the permanganate-oxalate reaction. *J. Am. Chem. Soc.* 1955, 77, 2036–2042.
- (69) Wright, M. H.; Geszvain, K.; Oldham, V. E.; Luther, G. W., III; Tebo, B. M. Oxidative formation and removal of complexed Mn (III) by Pseudomonas species. *Front. Microbiol.* **2018**, *9*, 560.
- (70) Zhang, H.; Huang, C.-H. Oxidative transformation of triclosan and chlorophene by manganese oxides. *Environ. Sci. Technol.* **2003**, *37*, 2421–2430.
- (71) Shareef, A.; Angove, M. J.; Wells, J. D.; Johnson, B. B. Aqueous solubilities of estrone, 17β -estradiol, 17α -ethynylestradiol, and bisphenol A. *J. Chem. Eng. Data* **2006**, *51*, 879–881.
- (72) Bhatnagar, A.; Anastopoulos, I. Adsorptive removal of bisphenol A (BPA) from aqueous solution: A review. *Chemosphere* **2017**, *168*, 885–902.
- (73) Butt, H.-J.; Graf, K.; Kappl, M. Physics and chemistry of interfaces; John Wiley & Sons Press, 2013.

- (74) DiStefano, V. H.; McFarlane, J.; Anovitz, L. M.; Stack, A. G.; Gordon, A. D.; Littrell, K. C.; Chipera, S. J.; Hunt, R. D.; Lewis, S. A., Sr.; Hale, R. E.; Perfect, E. Extraction of organic compounds from representative shales and the effect on porosity. *J. Nat. Gas Sci. Eng.* **2016**, *35*, 646–660.
- (75) Li, F.; Wang, J.; Jiang, B.; Yang, X.; Nastold, P.; Kolvenbach, B.; Wang, L.; Ma, Y.; Corvini, P. F.-X.; Ji, R. Fate of tetrabromobisphenol A (TBBPA) and formation of ester-and ether-linked bound residues in an oxic sandy soil. *Environ. Sci. Technol.* **2015**, *49*, 12758–12765.
- (76) Fent, G.; Hein, W. J.; Moendel, M. J.; Kubiak, R. Fate of ¹⁴C-bisphenol A in soils. *Chemosphere* **2003**, *51*, 735–746.
- (77) Agenson, K. O.; Oh, J.-I.; Urase, T. Retention of a wide variety of organic pollutants by different nanofiltration/reverse osmosis membranes: controlling parameters of process. *J. Membr. Sci.* **2003**, 225, 91–103.
- (78) Huang, Q.; Weber, W. J. Transformation and removal of bisphenol A from aqueous phase via peroxidase-mediated oxidative coupling reactions: efficacy, products, and pathways. *Environ. Sci. Technol.* **2005**, 39, 6029–6036.
- (79) Stafiej, A.; Pyrzynska, K. Adsorption of heavy metal ions with carbon nanotubes. *Sep. Purif. Technol.* **2007**, *58*, 49–52.
- (80) Ahmad, B. J.; Cheng, W.; Low, W.; Nora'aini, A.; Noor, M. M. M. Study on the removal of iron and manganese in groundwater by granular activated carbon. *Desalination* **2005**, *182*, 347–353.
- (81) Massa, W.; Yakubovich, O. V.; Dimitrova, O. V. A novel modification of manganese orthophosphate Mn₃(PO₄)₂. *Solid State Sci.* **2005**, *7*, 950–956.
- (82) Ren, X.; Santamarina, J. The hydraulic conductivity of sediments: A pore size perspective. *Eng. Geol.* **2018**, 233, 48–54.
- (83) Kuzyakov, Y.; Mason-Jones, K. Viruses in soil: Nano-scale undead drivers of microbial life, biogeochemical turnover and ecosystem functions. *Soil Biol. Biochem.* **2018**, *127*, 305–317.